Molecular Therapy
Original Article

lncRNA *HITT* inhibits metastasis by attenuating Rab5-mediated endocytosis in lung adenocarcinoma

Xingwen Wang,[1,4] Shanliang Zheng,[1,4] Fan Yang,[1] Wenxin Zhang,[1] Dong Zhao,[1] Xuting Xue,[1] Qingyu Lin,[1] Yunfei He,[2] Guohong Hu,[2] and Ying Hu[1,3]

[1]School of Life Science and Technology, Harbin Institute of Technology, Harbin, Heilongjiang Province 150001, China; [2]Shanghai Institute of Nutrition and Health, University of Chinese Academy of Science, 320 Yuyang Road, Shanghai 200031, China; [3]Shenzhen Graduate School of Harbin Institute of Technology, Shenzhen 518055, China

Endocytosis of cell surface receptors is essential for cell migration and cancer metastasis. Rab5, a small GTPase of the Rab family, is a key regulator of endosome dynamics and thus cell migration. However, how its activity is regulated still remains to be addressed. Here, we identified a Rab5 inhibitor, a long non-coding RNA, namely *HITT* (HIF-1α inhibitor at translation level). Our data show that *HITT* expression is inversely associated with advanced stages and poor prognosis of lung adenocarcinoma patients with area under receiver operating characteristics (ROC) curve (AUC) 0.6473. Further study reveals that both endogenous and exogenous *HITT* inhibits single-cell migration by repressing β1 integrin endocytosis in lung adenocarcinoma. Mechanistically, *HITT* is physically associated with Rab5 at switch I via 1248–1347 nt and suppresses β1 integrin endocytosis and subsequent cancer metastasis by interfering with guanine nucleotide exchange factors (GEFs) for Rab5 binding. Collectively, these findings suggest that *HITT* directly participates in the regulation of Rab5 activity, leading to a decreased integrin internalization and cancer metastasis, which provides important insights into a mechanistic understanding of endocytosis and cancer metastasis.

INTRODUCTION

Metastasis is responsible for more than 90% of cancer-related mortality and yet remains the most poorly understood component of cancer pathogenesis.[1] Derailed endocytosis was recently reported to be a key player in cancer progression.[2] Thus, unraveling the mechanisms underlying endocytosis is of crucial importance not only for our understanding of the pathology of cancer but also to provide promising prognostic biomarkers and therapeutic targets in metastatic cancers.

Endocytosis is a highly regulated cellular process facilitating the uptake of various cargos, such as membrane proteins and extracellular molecules.[3] Through endocytosis, internalized molecules are rapidly targeted to the early endosome, where they are further sorted to recycling endosomes to be recycled back to the plasma membrane or late endosomes for degradation.[3] As such, this event is essential in adjusting the numbers and the localizations of receptors at the cell surface and is involved in a wide array of fundamental cell biological processes, such as cell migration, apoptosis, and proliferation.

Integrins are known to constitute the principal adhesion receptors for the extracellular matrix (ECM) and also represent key molecules whose activities are regulated by the endocytotic system.[4] Temporal and spatial regulation of integrin trafficking offers an important mechanism by which integrin–ECM adhesion turnover is regulated, and thus also integrin signaling through the tight control of integrin availability at the cell surface.[4] There is compelling evidence that integrin trafficking is required for efficient cell migration and invasion, which are fundamental cellular behaviors contributing to cancer metastasis.[5] Among the diverse types of integrins, heterodimers containing β1 integrins have been implicated in the development of malignancy and the control of cell adhesion.[6] It is not surprising that elucidating the mechanisms underlying β1 integrin trafficking has become a major focus of research.

GTPases of the Rab family are primary regulators of vesicular trafficking pathways.[7] Among these, Rab5 is a master regulator of the early endocytic pathway and has been shown to be essential for membrane protein trafficking, including of β1 integrin.[8,9] Clinically, increased expression and activity of Rab5 is associated with cancer metastasis in breast,[8] lung,[8] and colon[10] cancers, among others. Like all Rab superfamily proteins, the function of Rab5 relies on the activity of a GTPase that is controlled by a switch between a GDP-bound off state and a GTP-bound on state. The GTP-GDP cycle is aided by GTPase-activating proteins (GAPs), while the GDP-GTP exchange reaction is highly regulated by guanine nucleotide exchange factors (GEFs).[11,12] In the GTP-bound on state, Rab5 exerts its effects

Received 18 May 2021; accepted 6 January 2022;
https://doi.org/10.1016/j.ymthe.2022.01.014.

[4]These authors contributed equally

Correspondence: Ying Hu, School of Life Science and Technology, Harbin Institute of Technology, Harbin, Heilongjiang Province 150001, China.
E-mail: huying@hit.edu.cn

by binding to various specific effector proteins—including cargo proteins, motor proteins, and tethering factors—leading to increased endocytosis and the elevated invasive capability of cancer cells.[8] Overexpression of wild-type (WT) or a constitutively activated (Q79L) mutant Rab5 in cancer cells maximally stimulates endocytosis, promoting β1 integrin internalization and cell migration.[8] In line with this idea, increased expression of Rab5 GEFs, such as RIN1,[13] and decreased expression of its GAPs, such as RN-tre,[14] both increase Rab5 activity and are related to metastasis in cancer patients. GEF/GAP-regulated Rab5 is a potential therapeutic target in cancer; however, the regulatory mechanisms behind the actions of GAPs and GEFs on the activity of Rab5 are not well understood.

Long non-coding RNAs (lncRNAs) are a group of RNA transcripts with limited protein-coding potential with lengths more than 200 nucleotides (nt). They used to be considered to be transcriptional noise; however, evidence is mounting that lncRNAs are essential in regulating multiple biological processes.[15] Therefore, it is not surprising that altered expression of lncRNAs has been connected with human diseases including cancer.[16] Interestingly, pathway enrichment analysis has identified endocytosis as a key enriched pathway of differently expressed microRNAs related to lncRNA *UCA1* in lung cancers.[17] Roles of lncRNAs in regulating Rab GTPase expression have also been reported recently. lncRNAs, such as *SNHG3*,[18] *SNHG1*,[19] *linc00152*,[20] and *HOTAIR*,[21] inhibit Rab family member expression by "sponging" specific microRNAs. lncRNA NEAT1 regulates endocytosis-related genes by binding with p300/CBP and subsequently inhibiting H2K27ac.[22] These findings imply that lncRNAs may be important players in Rab-related biological processes. However, whether or not lncRNAs are directly involved in the regulation of Rab GTPase activity remains to be unraveled.

We recently characterized a lncRNA named *HITT* (HIF-1α inhibitor at translation level),[23] which is also referred to as *linc00637* or *PPP1R13B-DT*. The expression of this lncRNA is reduced in multiple human cancer tissues. Mechanistic study has revealed that *HITT* inhibits cell growth and angiogenesis by suppressing HIF-1α synthesis.[23,24] HIF-1α is has been linked to metastasis and poor survival of cancer patients. It is thus reasonable to propose that downregulation of *HITT* may serve as a potential prognostic marker, at least in some types of human cancer. Indeed, The Cancer Genome Atlas (TCGA) database analysis revealed that downregulation of *HITT* is associated with poor prognosis of cancer patients, such as those with lung adenocarcinoma (LUAD) and rectal cancer.[23] Given that lung cancer is the most prevalent cancer worldwide and remains the leading cause of cancer-related death, and LUAD is a major pathological subtype of lung cancer,[25] we examined the role of *HITT* in cancer metastasis mainly in patients with LUAD. Notably, we found that *HITT* inhibited cell migration under normoxia, suggesting that a HIF-1α-independent pro-metastasis mechanism may exist. Further mechanistic study yielded evidence that *HITT* inhibits cell migration and cancer metastasis by directly interacting with the Rab5 small GTPase, blocking its interaction with GEFs and resulting in attenuated Rab5 GTPase activity and retarded β1 integrin internalization. Our findings provide a mechanistic understanding of how Rab5 activity is regulated and also how lncRNAs drive cancer cell motility by modulating endocytosis.

RESULTS

Downregulation of *HITT* is associated with poor prognosis of patients with LUAD

To understand the role of *HITT* in lung cancer metastasis, we first examined its expression levels in human lung cancer tissues by analyzing the Database: TCGA. The results showed that *HITT* expression had no obvious relationship with the clinical stages of LUADs and lung squamous cell carcinomas (LUSC; Figures S1A and S1B). In contrast, an inverse association between *HITT* expression and metastasis was observed in LUADs but not LUSC (Figures S1C and S1D). In line with these data, *HITT* downregulation was associated with poor outcomes of patients with LUAD but not of those with LUSC (Figures S1E and S1F). The prognostic value of *HITT* downregulation in LUAD was confirmed by analyzing an independent lung cancer cohort from the Database: TCGA (Figures S1G and S1H).

Furthermore, we bought a LUAD tissue array with different stages and overall survival information (n = 88 pairs). *HITT* expression was determined by fluorescence *in situ* hybridization (FISH). The fluorescence intensities were quantified by ImageJ. Remarkably, the levels of *HITT*, as indicated by fluorescence intensities, were significantly lower in tumors than in paired adjacent normal controls (Figures 1A and 1B). Consistent with the results obtained by analyzing the TCGA database, patients with reduced expression of *HITT* in primary tumors showed increased risk for the development of metastasis (Figure 1E) and a poor overall survival (Figure 1F), whereas other factors, such as age and sex, were not significantly associated with *HITT* expression (Figure S1I). In addition, we also found that reduced levels of *HITT* were associated with higher tumor, node, metastasis (TNM) stages and grades of LUAD (Figures 1C and 1D). Tumor stages, metastasis, and *HITT* expression were identified as significant prognostic factors through univariate and multivariate regression analysis (Table 1). On the basis of these data, we further evaluated the prognostic value of *HITT* using receiver operating characteristics curves. The data revealed that tumor stages, metastasis, and *HITT* expression with area under receiver operating characteristics curves (AUCs) of 0.719, 0.6935, and 0.6473, respectively (Figures 1G and 1H). The combination of *HITT* expression with TNM stage or metastasis, with AUCs of 0.7863 and 0.7647, respectively, was better as a prognostic factor than stage or metastasis alone (Figures 1G and 1H). Therefore, *HITT* downregulation is a potential marker of poor prognosis for patients with LUAD.

HITT inhibits cell motility, migration, and invasion

HITT was markedly reduced in LUAD cell lines compared with normal lung tissue controls (Figure 2A), which provided an ideal model with which to study *HITT* functions and mechanisms *in vitro* and *in vivo*. Given the significance of cell migration and invasion in cancer metastasis, the roles of *HITT* on these properties were investigated in independent LUAD cell lines. Remarkably, *HITT*

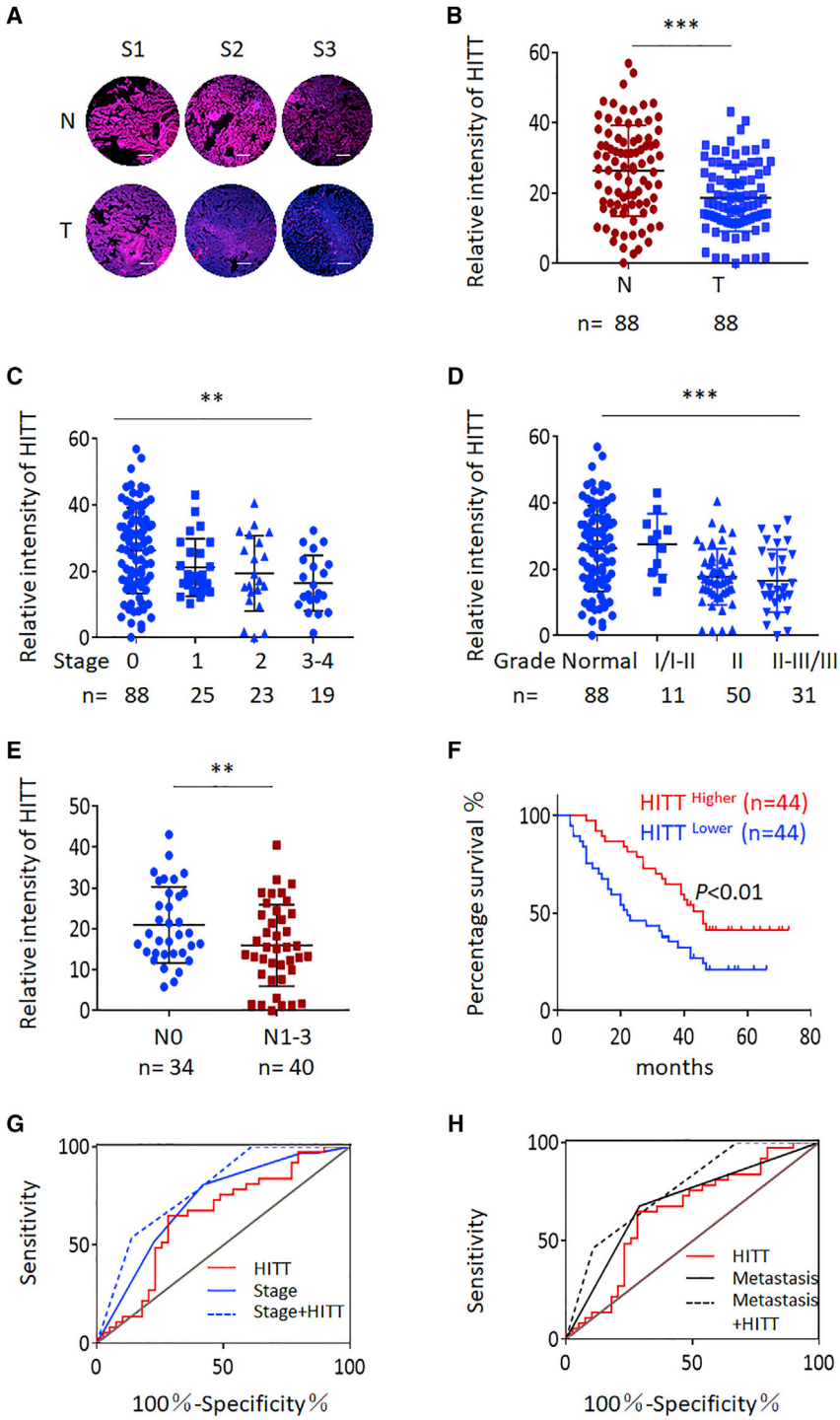

Figure 1. Downregulation of *HITT* is associated with poor prognosis of patients with LUAD

(A) Representative images of RNA-FISH staining of *HITT* in LUAD tissues (T) and paired adjacent normal controls (N). Red represents the *HITT* probe signal, and blue represents the nuclear signal. Scale bars in C and E, 50 μm. (B-E) *HITT* expression levels as indicated by the relative fluorescence intensity were compared between 88 cases of LUAD (T) and their adjacent normal controls (N) (n = 88, (B). Among those, samples having stage (n = 67), grade n = 92), and metastasis (n = 72) information were used to further analyze the association between *HITT* levels and stages (C) or grades (D) and metastasis status (N0, no lymph node metastasis; N1-3, lymph node metastasis, (E), respectively. (F) Kaplan-Meier overall survival curves of patients with LUAD stratified according to lower (below median value) and higher (above median value) expression levels of *HITT*. (G and H) ROC analysis for cancer-related survival of *HITT*, stage and metastasis alone (G and H), or the combination of *HITT* and stage (G) or *HITT* and metastasis (H). See also Figure S1.

overexpression in H292 cells (Figure 2B), a highly metastatic cell line with relatively low endogenous levels of *HITT*, dramatically decreased the cell migration and invasion rates, as revealed by wound healing, Boyden chamber, and Matrigel assays, respectively (Figures 2C and 2D). In contrast, *HITT* knockdown (KD) by two independent small interfering RNAs (siRNAs) in A549 cells (Figure 2B), a cell line with low-level metastasis that expresses relatively high levels of *HITT*, enhanced cell migration and invasion (Figures 2E and 2F). This was not due to changes in cell proliferation, because *HITT* had no obvious impact on it (Figure S2A).

We also found that migration speed was reduced 4.5-fold in cells overexpressing *HITT* and increased approximately 3-fold in *HITT* KD cells, as monitored by single-cell migration (Figures 2G and 2H). In addition, attachment and spreading on fibronectin-coated substrates was reduced by *HITT* expression and elevated by *HITT* KD (Figures 2I and 2J). These data collectively indicate that *HITT* plays essential roles in inhibiting cell migration and invasion, possibly by modulating the dynamic interactions between cells and the ECM. Furthermore, activity of *HITT* is likely to be common in human cancers, because *HITT* inhibited cell migration and spreading of cervical cancer HeLa and colon cancer HCT116 cells on fibronectin-coated substrates (Figures S2B–S2D).

HITT inhibits cell motility by blocking β1 integrin endocytosis

Next, we sought to investigate the underlying mechanisms by which *HITT* regulates cell motility. Adhesion signaling through integrins plays critical roles in modulating cell and ECM interaction and in regulating cell motility and invasion. As expected, blocking of integrin signals by ATN-161 or RGD peptides reduced cell migration. Remarkably, it also abolished the effects

Table 1. Univariate and multivariate regression analyses of parameters associated with the prognosis of LUAD patients

		Univariate analysis		Multivariate analysis	
Characteristic	Subset	HR (95% CI)	*p* Value	HR (95% CI)	*p* Value
Sex	Male/female	1.011(0.576–1.776)	0.97	1.261(0.634–2.506)	0.508
Age	≤60/> 60 years	1.295(0.74–2.264)	0.365	1.485(0.782–2.821)	0.227
Tumor size	≤5cm^3/> 5cm^3	1.448(0.758–2.765)	0.262	0.651(0.271–1.561)	0.336
Tumor grade	Grade(1 + 2)/grade(3 + 4)	1.635(1.09–2.453)	0.018	1.364(0.732–2.54)	0.328
Tumor stage	I+II/III/IV	4.394(2.211–8.73)	<0.001	3.073(1.285–7.35)	0.012
Metastasis	Yes/no	3.589(1.827–7.049)	<0.001	2.301(1.008–5.253)	0.048
HITT	High/medium/Low	0.432(0.242–0.771)	0.004	0.462(0.231–0.925)	0.029

HR hazard ratio, 95% CI 95% confidence interval.

of *HITT* (Figures 3A and S3A). Therefore, *HITT* mainly acts by interfering with integrin signals.

Expression levels of β1 integrin have been associated with lymph node metastasis in lung cancers.[26] However, *HITT* did not affect β1 integrin expression at the protein level (Figures 3B and 3C). Integrin endocytosis is a major mechanism through which integrin is involved in the regulation of cell migration.[4,5] Therefore, we examined integrin endocytosis rates by measuring levels of membrane-associated β1 integrin. The assays consistently showed that *HITT* overexpression inhibited, whereas *HITT* KD promoted, internalization of β1 integrin, as revealed by cell fractionation (Figures 3B and 3C) and cell staining assays (Figure 3D). In addition, as shown via flow cytometry, *HITT* reduced levels of surface-labeled β1 integrin, whereas *HITT* KD had the opposite effect (Figures 3E and S3B). Further study revealed that these effects of *HITT* were predominantly due to impaired endocytosis rather than altered integrin recycling, because primaquine, an inhibitor of receptor recycling, significantly enhanced internalized β1 integrin, but it did not abolish the difference between internalization of β1 integrin, as revealed by a biotin-association assay (Figure 3F). Taken together, these results indicate that *HITT* regulates cell motility by inhibiting integrin endocytosis.

HITT attenuates integrin internalization through physical interaction with Rab5

lncRNAs can exert their functions through RNA-protein interactions. To gain insight into the mechanisms involved in *HITT*-mediated integrin endocytosis, we performed biotinylated RNA pull-down assays to identify potential *HITT*-binding proteins in HeLa and H292 cells. Components that have been shown to be important in integrin endocytosis, such as Rab1, Rab4, Rab5, Rab7, Rab11, Rab14, Rab21, Rab25, and clathrin, were examined. Our results showed that biotinylated *HITT* was able to form a complex with a key regulator of early endosomes, Rab5 (Figure 4A and Figure S4A). This association is likely Rab5 specific, as no detectable levels of other family members coprecipitated with *HITT* (Figures 4A and S4A) and no detectable interaction was obtained for clathrin either. Moderate association between β1 integrin and *HITT* was detected in biotinylated *HITT* sense precipitates (Figure 4A), suggesting that β1 integrin may also be able to form a complex with *HITT*.

UV-crosslinking and immunoprecipitation (CLIP) can determine direct RNA and protein interactions in cells and was used to explore the physical interactions between *HITT* and its potential binding partners, such as Rab5 and β1 integrin, *in vivo*. Our results revealed that Rab5, rather than β1 integrin, was the most important candidate for direct interaction with *HITT* (Figure S4B). The association of Rab5 with *HITT* was enhanced by *HITT* overexpression and decreased by *HITT* KD (Figures 4B and S4C), further supporting a specific interaction between Rab5 and HITT. Moreover, in an *in vitro* biotinylated RNA pull-down assay, recombinant GST-Rab5 displayed a specific interaction with biotinylated sense but not biotinylated antisense *HITT* (Figure 4C).

As shown above, *HITT* interacts with Rab5. We next explored the molecular nature of this interaction. First, different *HITT* fragments were generated and introduced into 4T1 cells, a cell line without endogenous *HITT* expression.[23] *HITT* are divided into three fragments (F1, F2, F3) according to its exon sequences. The interaction of Rab5 with exogenous *HITT* was determined by CLIP. The 3′ end of *HITT* (1030–2050 nt) contributed to the association with Rab5 (Figure 4D, top). The binding sequence was further mapped to 1248–1715 nt (Figure 4D, bottom). This was not due to differential expression levels of *HITT*, as similar *HITT* fragments were introduced into 4T1 cells (Figure 4D). The binding mechanism between *HITT* and Rab5 was also validated via an *in vitro* biotinylated RNA pull-down assay with purified GST-Rab5 (Figure 4E). In addition, *HITT*(1248–1715 nt) were truncated to a series of 100-nt fragments. Among them, *HITT* (1248-1347nt) was determined to be essential for Rab5 binding (Figure 4F). The optimal secondary structure with a minimum free energy was predicted by RNAfold web server (http://rna.tbi.univie.ac.at) (Figure 4G). Remarkably, this fragment was found to fold as independent loop structures in *HITT* (highlighted in red, Figure 4G). In support of these idea, we found that the sequence with the independent loop structures of *HITT* retains both Rab5 binding and Rab5 inhibitory abilities (Figure S4D).

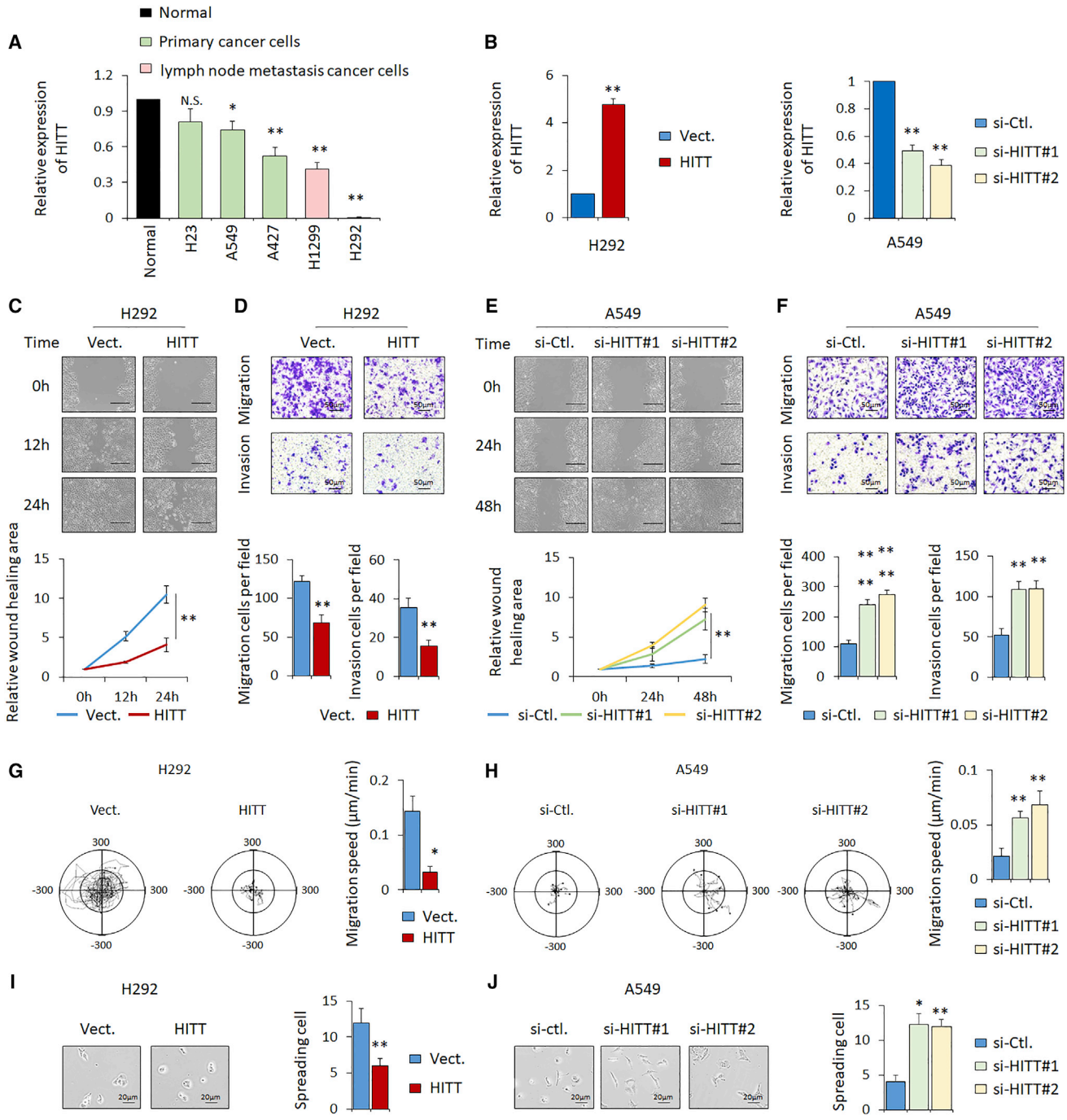

Figure 2. *HITT* inhibits cell motility, migration, and invasion

(A) The expression levels of *HITT* were determined by real-time qRT-PCR in LUAD cell lines and three pooled normal lung tissue controls. 18S was used as an internal control. (B) *HITT* overexpression or KD efficiency was confirmed by qRT-PCR in H292 and A549 cells, respectively. 18S was used as an internal control. Vect., vector. (C–F) Cell migration and invasion were determined by wound healing, Boyden chamber, and Matrigel assays in H292 cells after *HITT* overexpression (C and D) and A549 cell after *HITT* KD (E and F). Quantification of cell migrating and invasive abilities were presented in the bar graphs (bottom). Scale bars in C and E, 100 μm. Scale bars in D and F, 50 μm. Ctl., control. (G and H) Single-cell migrating ability was determined by random migration assay as shown in Materials and methods. Tracking images are shown (left) and the migration speeds of *HITT* overexpression H292 (G) and *HITT* KD A549 (H) cells were calculated and are presented in the bar graphs (right). n = 8/each group. (I and J) Representative images of cell spreading of *HITT* overexpression H292 (I) and *HITT* KD A549 (J) cells are presented (left), and quantification data are shown in a bar graph (right). Scale bar, 20 μm. The data derived from three independent experiments are represented as means ± SEM in the bar graph. Values in control cells were normalized to 1. **$p < 0.01$ (A–J). See also Figure S2.

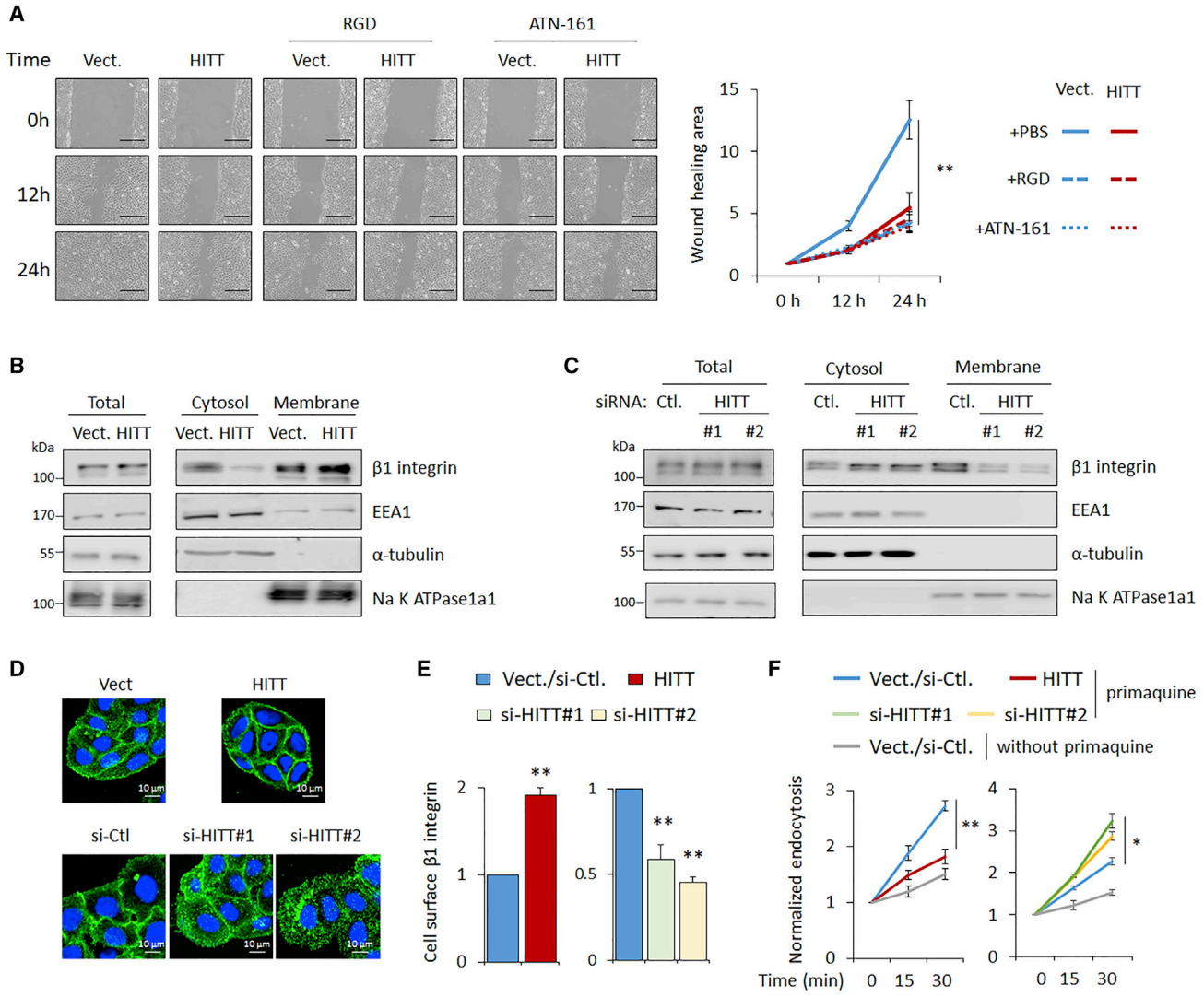

Figure 3. *HITT* inhibits cell motility by blocking integrin endocytosis

(A) Cell migrating ability was determined by wound healing assay in *HITT* ectopic expression H292 cells, in the presence or absence of ATN-161 or RGD (left), and quantification of cell migration is presented in the bar graph (right). Scale bar, 100 μm. (B–D) The localization of β1 integrin was determined by subcellular fractionation (B and C) and immunofluorescence (D) assays in *HITT* overexpression H292 (B and D) and *HITT* KD A549 cells (C and D). (E) Cell surface β1 integrin was determined by FACS in *HITT*-overexpressed H292 and *HITT* KD A549 cells. (F) The endocytosis rates of β1 integrin were measured by biotinylated internalization ELISA capture assays in *HITT*-overexpressed H292 and *HITT* KD A549 cells. The data derived from three independent experiments are represented as means ± SEM in the bar graph (A, E, and F). Values in control cells were normalized to 1. *$p < 0.05$; **$p < 0.01$; (A, E, and F). See also Figure S3.

Rab5 has been demonstrated to be required for β1 integrin internalization that coordinates cell migration. Interestingly, the effect of *HITT* on β1 integrin internalization was completely abrogated by Rab5 KD, but was unchanged by Rab21 KD (Figure 4H). In addition, only *HITT* fragments that were able to bind with Rab5 (1030–2050 nt and 1248–1715 nt) had effects on β1 integrin internalization (Figure 4I). Supportively, β1 integrin endocytosis is essential for focal adhesion dynamic, an important process in regulating cell migration. In line with above data, we also found that *HITT* inhibits focal adhesion disassembly in a Rab5-dependent manner by a nocodazole-based microtubule depletion assay (Figure S4E). In addition, although the factors, such as integrin-linked kinase (ILK), play a role in regulating integrin signaling, it has no impacts on *HITT*-regulated cell migration (Figures S4F and S4G). Therefore, *HITT* regulates β1 integrin endocytosis by physiologically associating with Rab5 via 1248–1715 nt.

The binding of *HITT* to Rab5 is required for its ability to inhibit Rab5 activity

The small GTPase activity of Rab5 is required for β1 integrin endocytosis.[27] Given the inhibitory effect of *HITT* on β1 integrin endocytosis

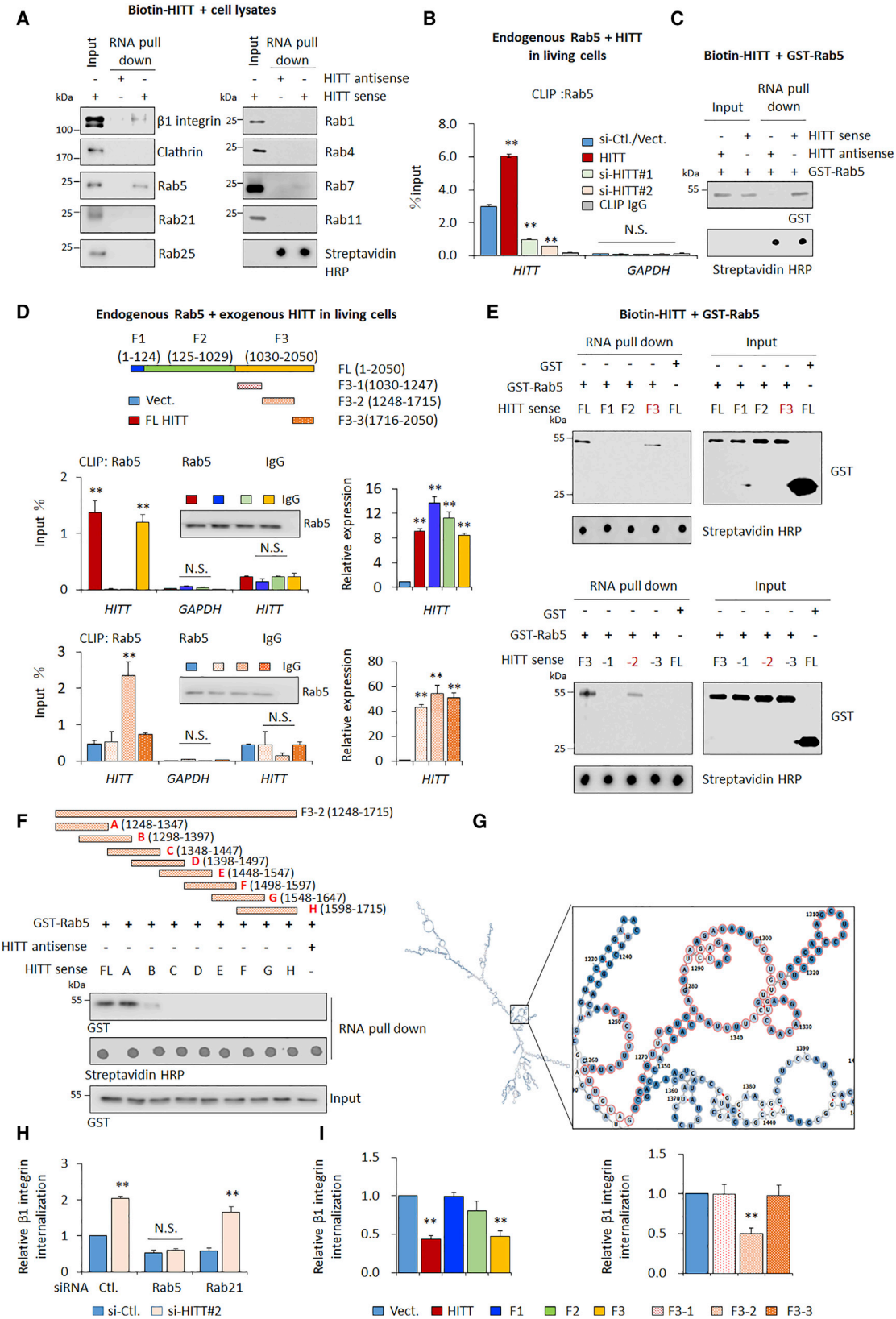

(legend on next page)

and its Rab5-dependent features (Figures 2–4), we reasoned that *HITT* may act by inhibiting the small GTPase activity of Rab5. In support of this hypothesis, GTP-(Q79L)-locked Rab5 reversed *HITT*-inhibited β1 integrin internalization more efficiently than WT Rab5, whereas GDP-(S34N)-locked Rab5 had no obvious effect on *HITT*-inhibited β1 integrin internalization (Figure S5).

To provide more direct evidence, the effects of *HITT* on Rab5 activity were explored via a well-established R5BD-GST pull-down assay. Rab GTPases in their GTP-bound active conformation bind with their effectors. Rabaptin5, a well-characterized Rab5 effector, was used as a template to synthesize the Rab5-binding domain (R5BD) with a GST tag, and the peptide was purified *in vitro*. GST-R5BD was mixed with cell lysates from *HITT*-overexpressing or -KD cells and subjected to a R5BD-GST pull-down assay. The results showed that *HITT* overexpression was inhibited, whereas siRNA-mediated *HITT* KD inhibition of *HITT* elevated Rab5 activity, as indicated by the co-precipitated Rab5 proteins in the GST-R5BD immunoprecipitates (Figure 5A). A similar inhibitory effect on Rab5 activity was observed for those *HITT* fragments (F3 and F3-2) that contained critical Rab5-binding sites (1248–1715) in the same assay (Figure 5B). Consistent with this, the reduced association of endogenous Rab5 and EE1A was validated by immunoprecipitation (IP) assays after *HITT* overexpression in HeLa cells, while *HITT* KD was found to increase the binding between Rab5/EE1A in the same assays (Figure 5C).

Moreover, Rab5 activity has been reported to change with microtubule dynamics. To test the biological significance of Rab5/*HITT* interaction in a more relevant biological model, the effects of *HITT* were compared after treating cells with nocodazole, a rapidly reversible inhibitor of microtubules. Consistent with previous reports, Rab5 activation, as shown in a R5BD-GST pull-down assay, was decreased after the disruption of microtubules with nocodazole but was restored rapidly after nocodazole washout (Figure 5D). The inhibition of Rab5 activity was more evident in *HITT*-overexpressing cells. The endocytosis of β1 integrin displayed the same kinetic changes as those observed for Rab5 activity in the same set of experiments (Figure 5E). In support of the biological significance of *HITT* and Rab5 interaction, levels of *HITT*-associated Rab5 were inversely related to Rab5 activity, as shown in CLIP assays (Figure 5F). These data collectively suggest that the interaction of *HITT* with Rab5 is required for its ability to inhibit Rab5 activation.

HITT inhibits Rab5 activity by blocking its interactions with its GEFs

Activation of Rab5 requires the activation of GEFs or the inactivation of GAPs. One would expect that *HITT* would either inhibit Rab5's association with its GEFs or facilitate its association with its GAPs. To test these hypotheses, the interactions of endogenous Rab5 with its best-known GEF and GAP (rabex5, Rin1, and RN-tre) were examined by IP assays in cancer cell lines containing different levels of *HITT*. We found that *HITT* overexpression significantly reduced co-precipitation of rabex5 and Rin1 with Rab5 (Figures 5G and S6A), whereas *HITT* KD enhanced its binding (Figure 5G). However, the interaction between Rab5 and RN-tre was not affected by *HITT* (Figure S6B). Thus, we reasoned that *HITT* may inhibit Rab5 activity by modulating the interaction between Rab5 and its GEFs. To validate this idea, we further evaluated the impacts of *HITT* on the binding between Rab5 and the Vps9 domain, an essential motif commonly found in the catalytic domains of Rab5 GEFs, *in vitro* (Figure S6C). As shown, *HITT* indeed inhibited the binding of recombinant Vps9 to Rab5. In addition, increasing amounts of *in vitro* synthesized biotinylated *HITT* competed with and displaced the binding (Figure 5H).

One potential explanation is that *HITT* binding may interfere with Vps9 binding to Rab5. If that is the case, GEFs and *HITT* may bind to similar regions on Rab5. To this end, biotinylated *HITT* was mixed with the same amounts of purified full-length Rab5 or Rab5 truncations. The *in vitro* biotinylated RNA pull-down assay revealed that the 1- to 73-aa) and 42- to 216-aa regions of Rab5, but not the 74- to 216-aa region, bound with *HITT*, suggesting that the 42- to 73-aa region of Rab5, containing switch I region (43–52 nt), is involved in binding (Figure 5I). Interestingly, it has been well established that the Rab5 switch I region contains critical residues for GEF binding.[28] These data suggest that *HITT* may affect the accessibility of switch I for GEF binding. These data collectively suggest that *HITT* inhibits Rab5 GTPase activity and thus Rab5-mediated β1 integrin internalization by inhibiting GEF binding.

HITT inhibits cell migration and cancer metastasis by inhibiting Rab5 activity

Because of its important function in regulating Rab5 activity and subsequent β1 integrin internalization, we reasoned that *HITT* might inhibit cell migration in a Rab5 activity-dependent manner. To this

Figure 4. *HITT* attenuates integrin internalization through physical interaction with Rab5

(A) β1 integrin, clathrin, Rab5, Rab21, Rab25, Rab1, Rab4, Rab7, and Rab11 levels in protein complexes immunoprecipitated by biotinylated *HITT* sense or antisense from whole-cell extracts of HeLa cells were determined by *in vitro* RNA pull-down assay combined with western blot (WB). The RNA pull-down efficiency was determined by streptavidin HRP. (B) Rab5-associated *HITT* was measured by Rab5 CLIP after *HITT* overexpression or KD in living HeLa cells. GAPDH mRNA and CLIP IgG were used as negative controls. (C) The binding of biotinylated *HITT* with recombinant GST-Rab5 was determined by biotinylated RNA pull-down assay *in vitro*. Biotinylated antisense HITT serves as a negative control. (D and E) CLIP (D) and biotinylated RNA pull down assay (E) were used to detect the binding of Rab5 with full-length or *HITT* fragments, as indicated in the diagram. Rab5 pull-down efficiency was determined by WB. (F) The interaction between biotinylated *HITT* truncates and GST-Rab5, as indicated in the diagram, were determined by biotinylated RNA pull-down assay. Biotinylated *HITT* antisense acts as a negative control. (G) Secondary structure of *HITT* was analyzed by RNAfold web server (http://rna.tbi.univie.ac.at). The red domain is Rab5-binding domain on *HITT*. (H and I) β1 integrin internalization was measured by biotinylated internalization ELISA capture assay after Rab21 KD, Rab25 KD (H), or *HITT* and *HITT* fragment overexpression (I) in HeLa cells. The data derived from three independent experiments are represented as means ± SEM in the bar graph (B, D, H, and I). Values in control cells were normalized to 1 (H and I). $^{**}p < 0.01$; N.S., not significant (B, D, H, and I). See also Figure S4.

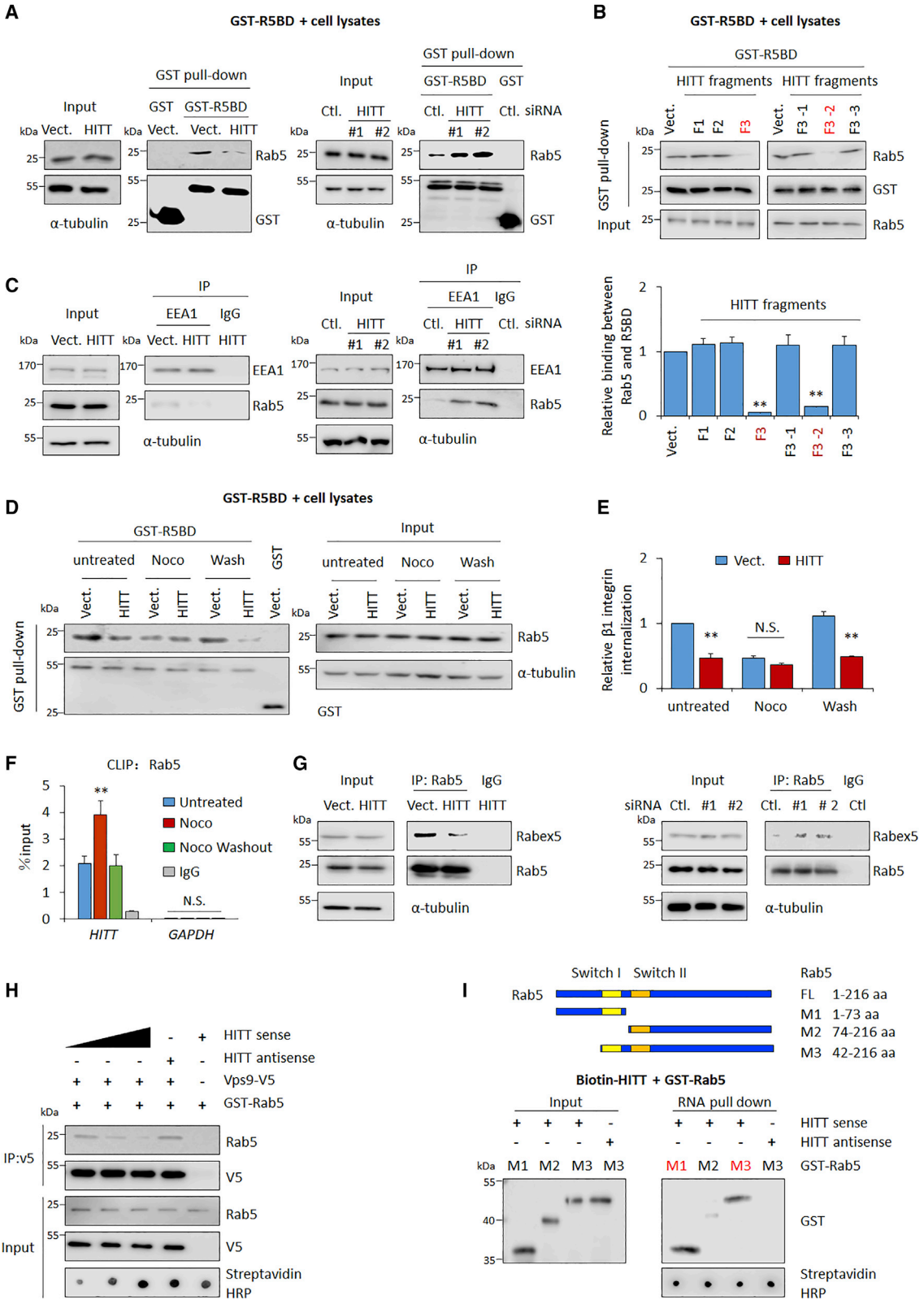

(legend on next page)

end, the effect of *HITT* on cell migration and invasion was compared after siRNA-mediated Rab5 KD. KD efficiency was confirmed by Western blot (Figure 6A). Under such conditions, Rab5 KD cells had weaker abilities to migrate, invade, and spread. The activity of *HITT* was missing after Rab5 KD (Figures 6B, 6C, S7A, and S7B). To provide further evidence, we also expressed v5-tagged WT Rab5, a GTP-locked Rab5 mutant (Q79L), and a GDP-bound Rab5 mutant (S34N) in *HITT*-overexpressing cells to similar levels (Figure 6D). The results revealed that WT Rab5 and the GTP-locked Rab5 mutant (Q79L), but not the GDP-bound Rab5 mutant (S34N), successfully rescued the capability of *HITT* to influence cell migration. The effect of the GTP-locked Rab5 mutant was stronger than that of WT Rab5 (Figures 6E and 6F). These data collectively suggest that *HITT*'s regulation of cell migration and invasion is dependent on its ability to inhibit Rab5 GTPase activity.

To verify the effect of *HITT* on cancer metastasis *in vivo*, A549 cells were engineered to stably express luciferase together with either *HITT* or CRISPR/Cas9-*HITT*. The same numbers of A549 clones were injected into nude mice through tail vein injection, and the metastatic status of A549 cells was monitored weekly by bioluminescence imaging. As shown, *HITT* knockout strongly promoted the colony-forming ability of A549 cells in the lung (Figures 7A and 7B), which are normally not highly invasive. Eight weeks after injection, increased lung metastasis after *HITT* knockout was further confirmed by *ex vivo* bioluminescence imaging (Figures 7C and 7D) and hematoxylin and eosin (H&E) staining (Figure 7E). In contrast, *HITT* overexpression repressed lung metastasis and the number of metastatic lung nodules, as shown by *in vivo* (Figures 7F and 7G) or *ex vivo* (Figures 7H and 7I) bioluminescence imaging and H&E staining (Figure 7J), respectively. In accord with our observations *in vitro*, the activity of Rab5 was inhibited by *HITT* knockout (Figure 7K) and decreased by *HITT* overexpression in the animal models (Figure 7L).

Further studies also revealed that the ability of *HITT* to inhibit cancer metastasis was mainly dependent on its ability to repress Rab5 GTPase activity. The inhibitory effect of *HITT* overexpression on cancer metastasis was partially reversed by WT Rab5 and completely abolished by the GTP-locked Rab5 mutant (Q79L) but not affected by the GDP-bound Rab5 mutant (S34N) (Figures 7F–7J). This was not due to different expression levels of Rab5, since similar levels of exogenous v5-tagged Rab5 WT or mutant proteins were detected by Western blot using anti-Rab5 or anti-v5 tag antibody (Figure 7L).

DISCUSSION

Metastasis remains the greatest challenge in the clinical management of cancer.[29] Rab5 is a primary regulator of the vesicular trafficking pathways and has attracted interest as a key regulator of cancer metastasis.[8] Elucidation of the regulatory mechanisms of Rab5 may provide important insights into cancer metastasis. Up to now, many reports have demonstrated that Rab5 activity is regulated by GEFs and GAPs,[30] however, the detailed mechanisms by which their interactions are modulated remain poorly understood. An increasing number of lncRNAs has been reported recently.[31,32] Our study establishes a lncRNA to be an inhibitor of Rab5, which acts by directly interacting with Rab5 and inhibiting the binding with its GEFs. To the best of our knowledge, this is the first evidence of a lncRNA binding with a GTPase and directly regulating GTPase activity and endocytosis pathways.

Given the essential and highly dynamic regulatory roles played by Rab5 in fundamental biological processes, it is not surprising that multiple layers of regulation exist to guarantee tight and precise control. Our data suggest that *HITT* serves as a Rab5 inhibitor by interfering the binding of Rab5 with its GEFs based on the following observations. First, binding with *HITT* reduced the interaction between Rab5 and its GEFs both *in vivo* and *in vitro*. Second, *HITT* binds with Rab5 at switch I, which also contributes to its binding with its GEFs. Third, increasing doses of *HITT* gradually substitute Vsp9 (an essential motif commonly found in the catalytic domains of Rab5 GEFs) in binding with Rab5 *in vitro*. Those observations motivated our hypothesis that *HITT* binding might enable residues, primarily in switch I, to adopt a conformation that prevents GEF proteins from loading (Figure 8). It has been proposed that It has been reported recently that the ubiquitination of Rab5 GEF Rebex-5[33] or Vps9,[34] and the association of Rab5 GEF Gapex5 with the adaptor protein SPIN90,[35] increases Rab5 activity by promoting the localization of GEFs to the early endosome. Our study provides a distinct mechanism through which the accessibility of Rab5 with its GEFs can be changed; combined with the findings of others, this suggests that cells utilize multiple strategies to precisely control Rab5 activity.

It is also worthwhile considering that the mechanisms of *HITT* and GEFs in binding with Rab5 may be somewhat different. In line with this idea, in contrast to the binding with its GEFs, there is an inverse relationship between Rab5/*HITT* interaction and Rab5 activity after nocodazole shock. In addition, *HITT* selectively binds with Rab5,

Figure 5. *HITT* inhibits Rab5 activity by blocking the interaction of Rab5 with it GEFs

(A and B) The activity of Rab5 was determined by R5BD GST pull-down assay after *HITT* overexpression or KD (A) or *HITT* fragments overexpression (B). The binding levels in the Vect. group were normalized to 1 (B, bottom). (C) The interaction between Rab5 and EEA1 was determined by a immunoprecipitation (IP) assay in *HITT*-overexpressed and KD cells. IgG was used as a negative control. (D–F) The activity of Rab5, β1 integrin internalization and Rab5/*HITT* interaction were measured by R5BD GST pull-down assay (D), biotinylated internalization ELISA capture assay (E), and CLIP (F) assays, respectively, in HeLa cells with or without *HITT* overexpression after treatment with nocodazole (Noco) or washout. (G) The interaction between Rab5 and Rabex5 was determined by IP assay in *HITT*-overexpressed and KD cells. IgG was used as a negative control. (H) *In vitro* synthesized Vps9-V5 and GST-Rab5 were mixed with 0, 1, or 2 μg of *HITT* sense or 2 μg of *HITT* antisense, respectively. The interactions between Vps9 and Rab5 were determined by IP assay. Biotinylated *HITT* antisense acts as a negative control. (I) The interactions between biotinylated *HITT* and GST-Rab5 or GST-Rab5 truncates, as indicated in the diagram, were determined by biotinylated RNA pull-down assay. Biotinylated *HITT* antisense acts as a negative control. The data derived from three independent experiments are represented as means ± SEM in the bar graph (B ,E, and F). Values in control cells were normalized to 1 (B and E). $^{**}p < 0.01$; N.S., not significant; (B, E, and F). See also Figure S5.

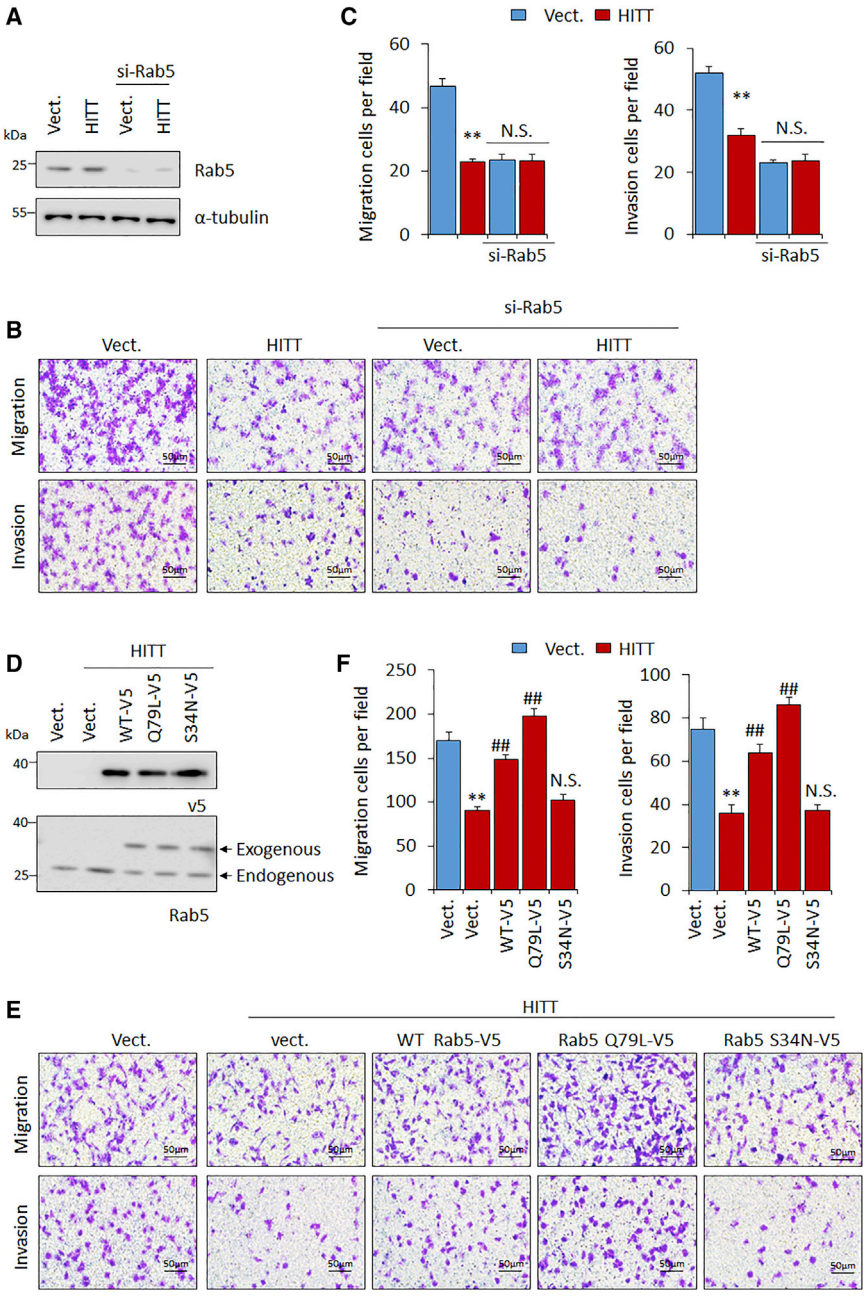

Figure 6. *HITT* inhibits cell migration and invasion by inhibiting Rab5 activity *in vitro*

(A) Rab5 KD efficiency was verified by WB in A549 cells. α-Tubulin acts as a negative control. (B and C) Cell migration and invasion were measured by Boyden chamber and Matrigel assays, respectively, in *HITT*-stably-expressed A549 lines and the corresponding vector controls with or without Rab5 KD (B). The quantification of cell migration and invasion is presented in the bar graph (C). (D) Overexpression efficiency of v5-tagged Rab5 WT, Q79L, and S34N in *HITT*-stably expressed A549 lines was verified by WB. (E and F) Cell migration and invasion were analyzed by Boyden chamber and Matrigel assays in A549 stable lines as indicated (E). The quantification of cell migration and invasion is presented in the bar graph (F). Data are derived from three independent experiments and represented as means ± SEM in the bar graphs. Values in control cells were normalized to 1. $^{**}p < 0.01$; compared with vect. (C and F). $^{\#\#}p < 0.01$; N.S., not significant, relative to the *HITT* overexpression or si-Rab5 control (C and F).

whereas Vps9-domain containing GEFs have been shown to bind both Rab5 and Rab21.[28] The selectivity of *HITT* in binding with Rab family members indicates a potential application of *HITT* to specifically inhibit Rab5 but not other Rabs. Further research is needed to compare the precise mechanisms of *HITT* and GEFs in binding with Rab5, possibly through structural biology approaches.

Furthermore, despite the model proposed above, we cannot exclude the possibility that *HITT* inhibits Rab5 GTPase activity *per se*. *HITT* binds via key nucleotides mapped to residues 42–73, which overlap with the switch I (residues 43–52) region and are proximal to the switch II (residues 77–95) region, regions that also constitute key structures of Rab5 involved in binding with nucleotides, in addition to GEFs.[36] Recent evidence has shown that modulating Rab5 protein via monoubiquitination at K165 reduces GDP release by changing its conformation at switch I, leading to reduced Rab5 activity.[37] Our data raise the possibility that HITT binding could cause a conformational change in switch I and switch II, which may result in preferential binding of Rab5 with GDP rather than GTP. This hypothesis is worthy of further exploration.

HITT is a recently identified lncRNA. The gene plays essential roles in regulating HIF-1α expression[23] and ATM activity[38] and therefore participates in the regulation of angiogenesis and the DNA damage response. In this study, for the first time, we have delineated the critical role of *HITT* in regulating cell migration and invasion. More importantly, this event is likely clinic relevant: expression levels of *HITT* are reduced in lung cancer. In addition, this study has investigated the potential of *HITT* expression in estimating the prognosis of patients with LUAD, supporting the idea that *HITT* expression has prognostic potential. Notably, *HITT* expression has a similar ability to predict overall survival at tumor grade and TNM stage but provides extra information on molecular pathology, suggesting that the assessment of *HITT* expression in patients might be a more straightforward and practical procedure. Furthermore, we found that *HITT* inhibits cancer metastasis in a Rab5 activity-dependent

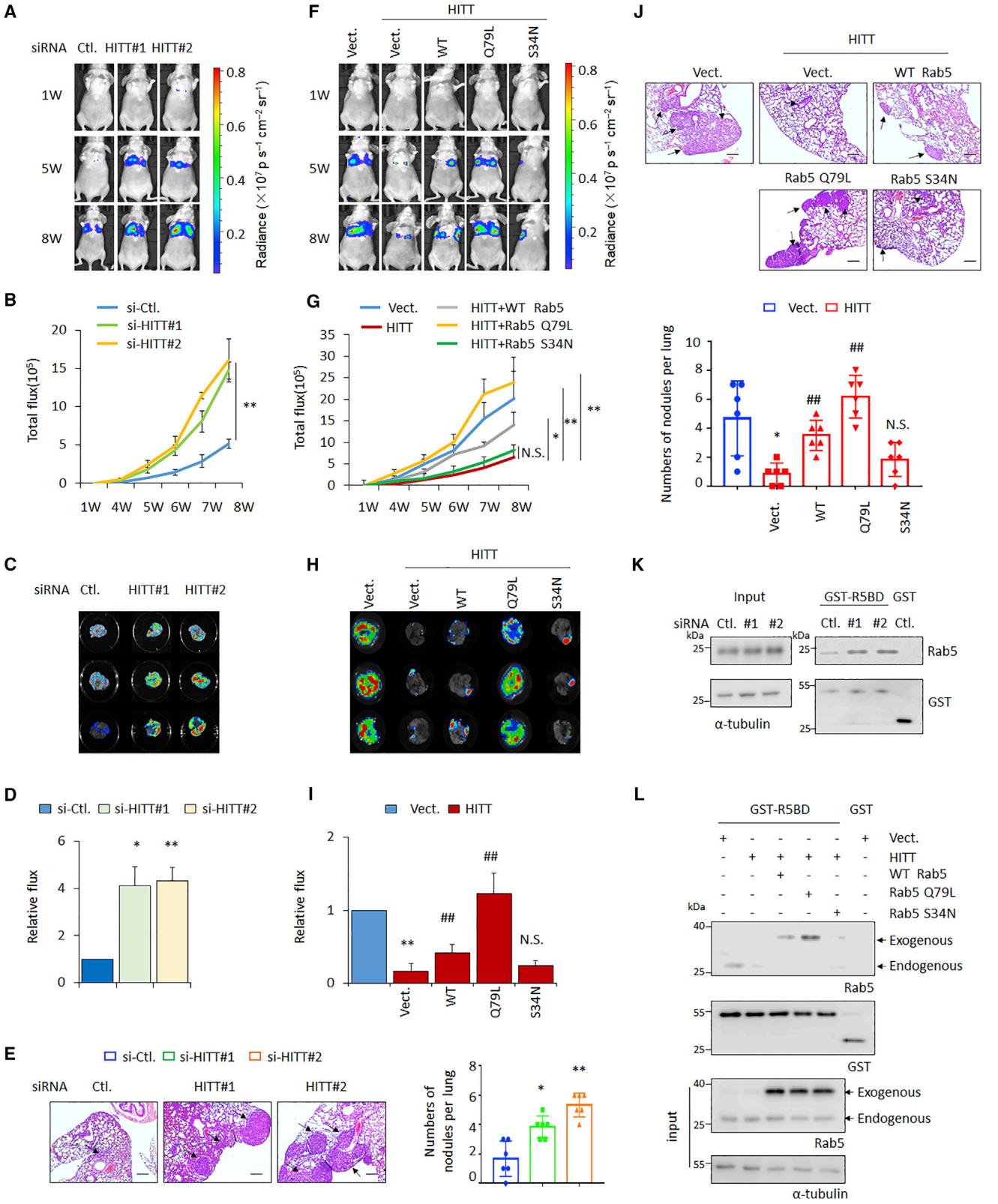

(legend on next page)

manner both *in vitro* and *in vivo*, implying that the anti-metastatic function of *HITT* in patients with LUAD may be related to Rab5 inactivation. Further validation of the inverse association between *HITT* expression and Rab5 activity in fresh LUAD tissue is needed. In addition, despite no inverse association being identified between *HITT* expression and tumor grade in the TCGA cohort (from the Nationwide Children's Hospital, USA), such an association was observed in the tissue array data (Shanghai, China). Whether or not *HITT* influences LUAD differentiation and, if so, whether or not it is human race specific need further investigation.

Genetic studies have revealed that Ras mutation is one of the most common genetic events in LUAC, and the presence of KRAS mutation is associated with unfavorable clinical outcome.[39,40] In addition, approximately 75% of LUACs examined harbor genetic alterations that promote the Ras signaling pathway.[41] Interestingly, several lines of evidence have indicated that Ras mutants exploit the endocytic machinery, at least in part by regulating Rab5,[42] suggesting that the dysregulation of Rab5 may be part of the downstream effects of increased Ras signaling. These data provide a potential explanation for *HITT*'s prognostic value in LUAC, but not in LUSC. It will be of interest to investigate whether *HITT*/Rab5 play essential roles in tumor types with defects in the Ras pathway in general.

Furthermore, in light of its critical role in regulating cancer metastasis, Rab GTPases are considered to be potential therapeutic targets in cancer.[43] In fact, several efforts have been made to inhibit the interaction between the GEFs and its G protein using small molecules.[44] However, this has been challenging due to the lack of a proper pocket for small-molecule binding. Our identification of a lncRNA inhibitor of the Rab5/GEF interaction provides important insights for the development of new anticancer therapies targeting Rab GTPases using RNA molecules, and therefore may be of clinical significance.

It is also noteworthy that Rab5 activity is required for multiple functions in addition to cell migration, such as mitophagy,[45] immunity,[46] and metabolism,[47] by binding to different effectors and regulating different cargo traffic. It will therefore be interesting to explore whether *HITT* plays roles in such contexts. In addition, KD of endogenous *HITT* results in increased activity of Rab5, suggesting that *HITT* plays essential roles in restricting intrinsic Rab5 activity in cells. Thus, *HITT* may be physiologically important, because it was reported recently that aberrant high activity of Rab5 is related to diseases such as Alzheimer's disease[48] and nephrotic syndrome.[49]

Taken together, our study reveals a distinctive mechanism by which Rab5 activity is regulated: a lncRNA *HITT* directly binds with Rab5 and interferes with the interaction of Rab5 with its GEFs. As such, *HITT* elicits a robust effect in inhibiting cancer metastasis, serves as a good prognostic marker, and is a potential therapeutic target for the prevention and treatment of LUAC metastases. The study enhances not only our understanding of the Rab5-mediated endocytic mechanism but also of how a small GTPase can be specifically targeted by a RNA molecule.

MATERIALS AND METHODS

Cell lines and treatments

The human lung cancer A549, H292, H1975, H1299, A427, H23, colorectal cancer HCT116, and cervical cancer HeLa cells were cultured in RPMI 1640 medium (GIBCO) or Dulbecco's modified Eagle's medium (DMEM) supplemented with 10% (v/v) fetal bovine serum (Biological Industries). All cells were grown at 37°C in a humidified incubator with 5% CO_2. All cell lines were authenticated and characterized by the supplier and were monitored regularly for their authenticity by the Genetic Testing Biotechnology Corporation (Suzhou, China) and to be free of mycoplasma contamination.

Tissue microarray and RNA-fluorescence *in situ* hybridization

Paraffin-embedded human tissue microarray containing 88 pairs of matched LUAD and corresponding normal control tissues (HLugA180Su03) were purchased from Shanghai Biochip (Shanghai, China). For the FISH assay, the tissue microarray was deparaffinized in xylene and rehydrated in serial dilutions of ethanol. After being washed in PBS for 5 min, the tissue microarray was treated with protein K at 37°C for 30 min. Next, the microarray was prehybridized in hybridization buffer (50% deionized formamide, 5× SSC, 5× Denhardt's, 250 μg/mL yeast tRNA, 500 μg/mL sperm DNA) at 37°C for 1 h. After that, the microarray was incubated with 200–300 ng/mL biotin-labeled anti-lncRNA *HITT* oligodeoxynucleotide probe at 37°C for 3 h. The microarray was then washed three times for 5 min each in 5× SSC, 2× SSC and 0.2× SSC at 37°C. After blocking in blocking buffer (10% milk dissolved in maleic acid buffer), the microarray was incubated in streptavidin Alexa Fluor 555 secondary antibody at room temperature for 1 h. DAPI was used as a nuclear counterstain. The fluorescence was measured with a laser scanning

Figure 7. *HITT* inhibits cancer metastasis by inhibiting Rab5 activity *in vivo*

(A and B) The representative bioluminescent imaging (A) and quantification of photon flux (B) of tumors in nude mice after intravenous injection of the control and CRISPR/Cas9-*HITT* A549 stable lines; n = 6 mice per group. (C–E) *In vitro* bioluminescent imaging (C), quantification of photon flux (D), representative H&E stain images (E, left), and the numbers of metastatic nodules (E, right) in the dissected lungs 8 weeks after intravenous injection of the control and CRISPR/Cas9-*HITT* A549 stable lines. Scale bar, 100μm. (F and G) The representative bioluminescent images (F) and quantification of photon flux (G) of tumors in nude mice after intravenous injection of the same number of A549 sub-lines as indicated; n = 6 mice per group. (H–J) *In vitro* bioluminescent imaging (H), quantification of photon flux (I), H&E stain images (J, top), and the numbers of metastatic nodules (J, bottom) in the dissected lungs 8 weeks after intravenous injection of vector controls or *HITT*-stably overexpressed A549 cells with or without Rab5 WT, Q79L, and S34N overexpression. Scale bar, 100μm. (K and L) The activity of Rab5 was determined by R5BD GST pull-down assay in genetically modified A549 xenografts as indicated. Data are represented as means ± SEM in the bar graphs. *$p < 0.05$. **$p < 0.01$; compared with Vect. or si-Ctl. (B, D, E, G, I, and J). ##$p < 0.01$; N.S., not significant, relative to the HITT overexpression (I and J).

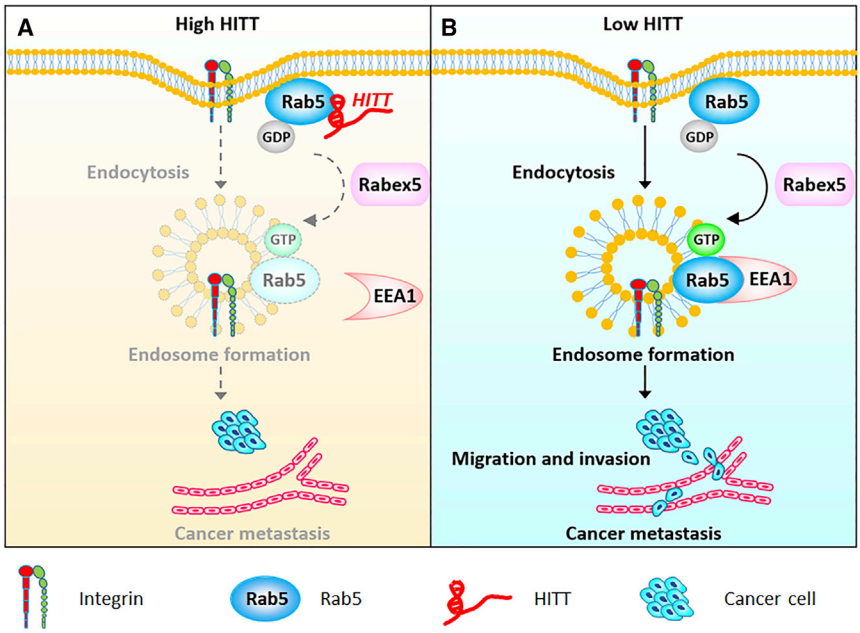

Figure 8. Proposed model for the modulation of small GTPase activity of Rab5 by lncRNA *HITT*

HITT, through its 1248–1715 nt, directly binds with Rab5 at (42–73 nt), a region involved in switch I. Switch I is a region that contains key residues that contribute to the binding with its GEFs, such as Rabex5. As such, *HITT* interferes with the interaction between Rab5 and its GEFs, resulting in a reduced small GTPase activity of Rab5, repressed β1 integrin , and attenuated cancer metastasis (A). In contrast, when *HITT* expression is reduced, such as in cancers, the small GTPase activity of Rab5 is free of *HITT* inhibition, leading to an increased activity of Rab5, consequently promoting β1 integrin internalization, cell migration, invasion, and cancer metastasis (B).

confocal microscope (Zeiss LSM880 With Airyscan). The fluorescence signal was quantified by ImageJ software.

siRNA transfection and *HITT* overexpression infection

siRNA specifically targeting *HITT, Rab5, Rab21* and non-specific si-scramble control were synthesized by GenePharma (Suzhou, China). All transfection experiments were conducted by lipofectamine 2000 (Invitrogen) following the manufacturer's instructions. The siRNA sequences used in this paper are listed in Table S1. 293T cells were transfected with lentivirus constructs of PlncKP-Control or PlncKP-*HITT*, together with virus packing plasmids. 48 h post-transfection, the lentivirus supernatant was collected by centrifuge and used to infect the target cancer cells. Seventy-two hours after infection, antibiotics were added to select positive clones. Single clones with *HITT* overexpression were harvested for future analysis.

RNA extraction and quantitative RT-PCR

Total RNA was isolated using TRIzol Reagent (Invitrogen) following the manufacture's protocol. qRT-PCR was performed in triplicate with an Applied Biosystems Prism 7500 Fast Sequence Detection System, using TaqMan universal PCR master mix according to the manufacture's protocol (Applied Biosystems). Gene expression levels relative to 18S rRNA were calculated by gthe $2^{-\Delta\Delta CT}$ method. The primer sequences used in RT-PCR are listed in Table S2.

Western blot

Total proteins from cell lines were isolated by UREA buffer (8 M urea, 1 M thiourea, 0.5% CHAPS, 50 mM DTT and 24 mM spermine). Equal amounts of proteins were separated by sodium dodecyl sulfate-polyacrylamide gel electrophoresis (SDS-PAGE). After incubation with the indicated primary and secondary antibodies, signals were visualized by ECL. Membrane was then ready for scanning with the Image studio system. Protein quantification was conducted by ImageJ software. The antibodies used in this study are listed below: Rab5 (Abcam), Rab21 (Santa Cruz Biotechnology), Rab1 (ABclonal), Rab4 (ABclonal), Rab7 (ABclonal), Rab11 (ABclonal), Rabex5 (Santa Cruz Biotechnology), Rab25 (Santa Cruz Biotechnology), integrin β1 (Abcam), clathrin (Abcam), early endosomal antigen 1 (EEA1, Abcam), glutathione S-transferase (GST, ABclonal), Na-K-ATPase 1a1 (Proteintech), α-tublin (Proteintech), β-actin (Proteintech), GAPDH (Proteintech), goat anti-mouse IgG horseradish peroxidase (HRP, Abcam), and goat anti-rabbit IgG HRP (Abcam).

Wound healing assay

The 1×10^5 cells were seeded in 24-well plates and incubated at 37°C in 5% CO_2 for 24 h and subjected to serum starvation for an additional 24 h before making the wound. To avoid cell proliferation, cells were maintained in the serum-free medium throughout the experiment. Mechanical scratching was made using the fine end of sterile pipette tips. The plates were washed with 1× PBS three times and cultured with serum-free medium for the indicated period of time. The images were captured with an inverted microscope. The open area was quantified by ImageJ software. Relative wound healing area was calculated and presented in the line graph.

Boyden chamber and Matrigel assays

The 5×10^4 cancer cells were suspended in 150 μL of serum-free medium and then added to the upper chamber. A 500-μL medium supplemented with 10% serum was added to the bottom chamber as a chemoattractant. The 24-well Boyden chamber (8 μm, Corning) with (Matrigel assay) or without (Boyden chamber assay) Matrigel were incubated at 37°C for 24 h. After the non-migrating cells in the upper chamber were wiped off carefully with cotton swabs, the cells on the polycarbonate membranes were fixed with 4% paraformaldehyde and stained with 0.2% crystal violet (Sigma-Aldrich). The cells were counted in three random fields on each membrane.

Random migration assay

Time-lapse microscopy was used to monitor the random migration of cancer cells. Images were taken at an interval of 15 min for 24 h during random migration. Cells were tracked manually with the "manual tracking" ImageJ plugins, and tracks were analyzed with the free Chemotaxis and Migration Tool from Ibidi (Munich, Germany). Tracks of each cell (n = 8) were produced and used to calculate average velocity according to the length/time, change in length over time.

Cell spreading assay

The 24-well culture plates were coated with fibronectin at 4°C overnight (Sigma-Aldrich) at a concentration of 2 μg/mL and then blocked with 2% BSA. Trypsinized cells were re-suspended in serum-free medium, and the same number of the suspended cells were seeded immediately on the top of fibronectin-coated culture plates. Cells were maintained in the incubator at 37°C for 4 h to allow cell spreading. Cells were washed by gentle wash in serum-free medium, and spreading cells were scanned using the inverted microscope (Lycra). Spreading cells were counted as cells with extended processes that were larger than one-half of the cell diameter, and non-spreading cells were defined as being refractive and round. The attached and spreading cells were counted in three random fields in each well.

Subcellular fractionation

Cells were lysed in hypotonic buffer (42 mM KCl, 10 mM HEPES [pH 7.4], 5 mM $MgCl_2$, 10 μg/mL each aprotinin and leupeptin) for 15 min on ice. Cells were transferred to a 1-mL syringe and repeatedly blown 30 times. The cell lysates were centrifuged at 200 × *g* for 10 min to remove nuclei and cell debris, and the supernatant was centrifuged at 13,000 × *g* for 60 min at 4°C. The supernatant (cytosol) was collected, and the pellet was resuspended in lysis buffer (20 mM Tris-HCl [pH 7.5], 150 mM NaCl, 1% NP-40, and 10 μg/mL each aprotinin and leupeptin), vortexed for 5 min at 4°C, and centrifuged at 13,000 × *g* for 60 min at 4°C. The supernatant (membrane) fraction was collected. Each fraction was boiled at 100°C for 5 min in SDS loading buffer and then subjected to western blot analysis.

Immunofluorescence assay

Cells grown on coverslips in a 24 well plate were fixed in 4% paraformaldehyde solution for 20 min after three washes in 1× PBS. After another round of washes in 1× PBS, cells were permeabilized with 0.1% Triton X-100 solution on ice for 4 min. The permeabilization solution was then removed by adding 1× PBS, following which cells were blocked in 3% BSA (Sigma-Aldrich) for 1 h. Incubation with the primary antibody was performed overnight at 4°C, followed by three washes in 1× PBS for 5 min each. Cells were then incubated with the fluorescently labeled secondary antibody for 1 h. After the cells had been washed three times with 1× PBS, DAPI was used for 5 min as a nuclei counterstain. The images were captured by a Zeiss LSM880 With Airyscan.

Cell-surface β1 integrin analysis by fluorescence-activated cell sorter

Cells were harvested and fixed in cold 4% paraformaldehyde solution for 10 min. After three washes in 1× PBS, cells were incubated with anti-β1 integrin (P5D2) mouse monoclonal antibody at room temperature for 1 h and washed three times in 1× PBS. After that, cells were incubated with FITC-conjugated second antibody for 1 h followed by the washes with PBS. Analyses were then performed on FACScan (BD Biosciences).

Biotinylated β1 integrin internalization and ELISA capture assay

Serum-starved (30 min) cells were washed twice in cold PBS, and surface labeled with 0.2 mg/mL NHS-SS-biotin (Thermo Fisher Scientific) in PBS at 4°C for 30 min. Labeled cells were washed twice in cold PBS and transferred to DMEM containing 1% FBS and 0.2 mM primaquine to allow internalization at 37°C for the times indicated. After two washings in ice-cold PBS, the biotin was removed from the protein remaining at the cell surface by incubation in a solution containing 20 mM MesNa in 50 mM Tris (pH 8.6) and 100 mM NaCl for 1 h at 4°C. After that, MesNa was quenched with 20 mM iodoacetamide (IAA) for 10 min followed by washes in cold PBS. Cells were then lysed in lysis buffer (100 mM NaCl, 25 mM Tris, 1 mM Na_3VO_4, 0.5 mM EDTA, 1% Triton X-100, 5% glycerol, and protease inhibitors). The internalized biotinylated β1 integrin in the lysates were measured by ELISA capture assay. Briefly, 96-well plates were coated with 5 μg/mL β1 integrin antibodies at 4°C overnight and blocked in 0.05% Tween 20 and 5% BSA for 1 h at room temperature for future use. The same number of lysates were incubated with β1 integrin-coated 96-well plates at 4°C overnight. After four washes in 1× PBS, the plates were incubated with HRP-streptavidin secondary antibodies at 4°C for an additional 1 h in 1% BSA blocking solution. The relative levels of biotinylated β1 integrin were measured with a microplate reader.

RNA pull-down assay

Biotin-labeled RNA were synthesized with biotin RNA Labeling Mix (Roche). After treatment with RNase-free DNase I, biotinylated RNA was heated at 70°C for 15 min and then cooled down on ice for 2 min. Then secondary structure recovered biotinylated RNA reacted with streptavidin agarose beads (Invitrogen) at 4°C for 2 h. The fresh cell lysates or purified GST-fused proteins were collected and incubated with RNA-captured beads at 4°C for 1 h. Beads were briefly washed five times with washing buffer (50 mM Tris-HCl [PH 7.4], 150 mM NaCl, 1 mM $MgCl_2$, 0.05% NP-40). The resulting beads were boiled at 100°C for 5 min in SDS loading buffer and then subjected to western blot analysis.

UV-cross-linking RNA immunoprecipitation (CLIP)

The 1×10^7 cells were washed and UV cross-linked at 4.00 mJ/cm^2 and collected in in lysis buffer (5 mM PIPES[pH 8.0], 85 mM KCl, 0.5% NP-40) and 1% SDS, 10 mM EDTA, 50 mM Tris-HCl (pH 8.1) supplemented with protease inhibitor cocktail and RNase inhibitor (Thermo Fisher Scientific). After being precleared with protein A/G Sepharose beads, cell lysates were treated with the indicated antibodies or IgG control at 4°C overnight. Then, the antibody-RNA complexes were collected using the blocked protein A/G Sepharose beads. The immunoprecipitated RNA was eluted and isolated for the subsequent reaction to be reverse transcribed into first-strand

cDNA that would be used for further qRT-PCR analysis for the target RNA of interest.

Focal adhesion disassembly assay

Cells were grown on glass coverslips and serum starved for 12 h prior to treatment with 10 μM nocodazole for 1 h to completely depolymerize microtubules. Nocodazole was washed away and replaced with serum-free medium and, at the indicated times, cells were fixed in paraformaldehyde, permeabilized, and immunostained with the indicated antibodies.

R5BD GST pull-down

Rab5-binding domain (R5BD) of Rabaptin5 was cloned into the pGEX-6p-1 vector. On the one hand, GST-R5BD produced in bacterial cells was subsequently purified with glutathione Sepharose beads (Beyotime Biotechnology). On the other hand, the indicated targeting cancer cells were washed with ice-cold PBS and lysed in NETN buffer (50 mM Tris-HCl [pH 8.0], 150 mM NaCl,1% NP-40,1 mM EDTA). Cell lysates were clarified by centrifugation at 16,000 × *g* for 25 min at 4°C. The GTP-bound Rab5 is able to bind with GST-R5BD. To this end, 500 μL of supernatant was incubated with 20 μL of purified GST-R5BD protein combined with the glutathione Sepharose beads for 1 h at 4°C on a rotating mixer. After reaction, the beads were boiled at 100°C for 5 min in SDS loading buffer and subjected to wWestern blot analysis with the anti-Rab5 antibody.

Immunoprecipitation

Cells were lysed in NETN buffer (50 mM Tris-HCl [pH 8.0], 150 mM NaCl,1% NP-40,1 mM EDTA), adding proteinase inhibitor cocktail (MedChemExpress) freshly before use. The lysate was than precleaned with protein A/G Sepharose beads (GE Healthcare), and specific antibodies or control IgG was added to supernatant and incubated with blocked beads at 4°C overnight. Beads with the bound immunoprecipitates were collected and washed four times with the cold NETN buffer, and then proteins were analyzed for western blot assay.

Xenografted tumor model *in vivo*

The female nude mice between 4 and 5 weeks old were purchased from Beijing HFK Bioscience. A549 cells were engineered to stably express luciferase together with either *HITT* or CRISPR/Cas9-*HITT*. *HITT*-overexpressed cells infected with lentivirus constructs of Rab5 (WT), Rab5 (Q79L), and Rab5 (S34N). The same numbers (1×10^6 or 2×10^6) of A549 clones were injected into nude mice through tail vein injection. The metastatic status of A549 cells that were stably labeled with a firefly luciferase was monitored weekly by bioluminescence imaging (BLI). After 8 weeks, the mice were anesthetized and euthanized. The removed tumor tissues were immediately stored in the liquid nitrogen or fixed in 4% paraformaldehyde before dehydration and embedding in paraffin. Paraffin sections were stained with H&E following the manufacture's procedures (Solarbio), and metastatic nodules in lungs were counted using microscope (Lycra). All animal procedures were performed according to protocols approved by the Rules for Animal Experiments published by the Chinese Government (Beijing, China) and approved by the Research Ethics Committee of Harbin Institute of Technology, China.

Statistical analysis

Statistical analysis was done with GraphPad software version 7. Data are presented as the means ± standard error of the means (SEM) or standard deviation (SD). Student's t test or $\chi 2$ test was applied to assess the statistical significance between two groups. ANOVA was used to assess the statistical significance among three groups or more. A p value < 0.05 was considered significant.

SUPPLEMENTAL INFORMATION

Supplemental information can be found online at https://doi.org/10.1016/j.ymthe.2022.01.014.

ACKNOWLEDGMENTS

This work was funded by the National Natural Science Foundation of China (Nos. 82025027, 82150115, 31871389, 31301131 and 320 00517), Basic Science Fundation of Science and technology innovation Commission in Shenzhen (No. JCYJ20170811154452255), China Postdoctoral Science Foundation (Nos. 2020M680045 and 2021 T140161), and the Nature Science Foundation of Heilongjiang Province (No. YQ2021C024).

AUTHOR CONTRIBUTIONS

Y.H. designed the experiments and wrote the paper. X.W. and S.Z. performed experiments and analyzed data for most figures. F.Y. did the RNA truncation studies. W.Z., D.Z., and Q.L. performed experiments and analyzed data for Figures S2A–S2D. X.X. generated truncated plasmids. Y.H. and G.H. generated luciferase expression A549 stable lines.

DECLARATION OF INTERESTS

The authors declare that they have no competing interests.

REFERENCES

1. Lambert, A.W., Pattabiraman, D.R., and Weinberg, R.A. (2017). Emerging biological principles of metastasis. Cell *168*, 670–691. https://doi.org/10.1016/j.cell.2016.11.037.

2. Mosesson, Y., Mills, G.B., and Yarden, Y. (2008). Derailed endocytosis: an emerging feature of cancer. Nat. Rev. Cancer *8*, 835–850. https://doi.org/10.1038/nrc2521.

3. Kaksonen, M., and Roux, A. (2018). Mechanisms of clathrin-mediated endocytosis. Nat. Rev. Mol. Cell Biol. *19*, 313–326. https://doi.org/10.1038/nrm.2017.132.

4. Moreno-Layseca, P., Icha, J., Hamidi, H., and Ivaska, J. (2019). Integrin trafficking in cells and tissues. Nat. Cell Biol. *21*, 122–132. https://doi.org/10.1038/s41556-018-0223-z.

5. Paul, N.R., Jacquemet, G., and Caswell, P.T. (2015). Endocytic trafficking of integrins in cell migration. Curr. Biol. *25*, R1092–R1105. https://doi.org/10.1016/j.cub.2015.09.049.

6. Blandin, A.-F., Renner, G., Lehmann, M., Lelong-Rebel, I., Martin, S., and Dontenwill, M. (2015). β1 integrins as therapeutic targets to disrupt hallmarks of cancer. Front. Pharmacol. *6*, 279. https://doi.org/10.3389/fphar.2015.00279.

7. Stenmark, H. (2009). Rab GTPases as coordinators of vesicle traffic. Nat. Rev. Mol. Cell Biol. *10*, 513–525. https://doi.org/10.1038/nrm2728.

8. Mendoza, P., Ortiz, R., Díaz, J., Quest, A.F.G., Leyton, L., Stupack, D., and Torres, V.A. (2013). Rab5 activation promotes focal adhesion disassembly, migration and

invasiveness in tumor cells. J. Cell Sci. *126*, 3835–3847. https://doi.org/10.1242/jcs.119727.

9. Mendoza, P., Díaz, J., Silva, P., and Torres, V.A. (2014). Rab5 activation as a tumor cell migration switch. Small GTPases *5*, e28195. https://doi.org/10.4161/sgtp.28195.
10. Díaz, J., Mendoza, P., Ortiz, R., Díaz, N., Leyton, L., Stupack, D., Quest, A.F.G., and Torres, V.A. (2014). Rab5 is required in metastatic cancer cells for Caveolin-1-enhanced Rac1 activation, migration and invasion. J. Cell Sci. *127*, 2401–2406. https://doi.org/10.1242/jcs.141689.
11. Cherfils, J., and Zeghouf, M. (2013). Regulation of small GTPases by GEFs, GAPs, and GDIs. Physiol. Rev. *93*, 269–309. https://doi.org/10.1152/physrev.00003.2012.
12. Bos, J.L., Rehmann, H., and Wittinghofer, A. (2007). GEFs and GAPs: critical elements in the control of small G proteins. Cell *129*, 865–877.
13. Tall, G.G., Barbieri, M.A., Stahl, P.D., and Horazdovsky, B.F. (2001). Ras-activated endocytosis is mediated by the Rab5 guanine nucleotide exchange activity of RIN1. Dev. Cell *1*, 73–82.
14. Palamidessi, A., Frittoli, E., Ducano, N., Offenhauser, N., Sigismund, S., Kajiho, H., Parazzoli, D., Oldani, A., Gobbi, M., Serini, G., et al. (2013). The GTPase-activating protein RN-tre controls focal adhesion turnover and cell migration. Curr. Biol. *23*, 2355–2364. https://doi.org/10.1016/j.cub.2013.09.060.
15. Kopp, F., and Mendell, J.T. (2018). Functional classification and experimental dissection of long noncoding RNAs. Cell *172*, 393–407. https://doi.org/10.1016/j.cell.2018.01.011.
16. Slack, F.J., and Chinnaiyan, A.M. (2019). The role of non-coding RNAs in oncology. Cell *179*, 1033–1055. https://doi.org/10.1016/j.cell.2019.10.017.
17. Chen, L., Cao, P., Wu, Q., Guo, Y., Yang, Y., and Chen, F. (2019). Overexpression of LncRNA-UCA1 correlates with lung adenocarcinoma progression and poor prognosis. Clin. Lab. *65*. https://doi.org/10.7754/Clin.Lab.2018.180739.
18. Zheng, S., Jiang, F., Ge, D., Tang, J., Chen, H., Yang, J., Yao, Y., Yan, J., Qiu, J., Yin, Z., et al. (2019). LncRNA SNHG3/miRNA-151a-3p/RAB22A axis regulates invasion and migration of osteosarcoma. Biomed. Pharmacother. *112*, 108695. https://doi.org/10.1016/j.biopha.2019.108695.
19. Wang, H., Wang, G., Gao, Y., Zhao, C., Li, X., Zhang, F., Jiang, C., and Wu, B. (2018). Lnc-SNHG1 activates the TGFBR2/SMAD3 and RAB11A/Wnt/β-catenin pathway by sponging MiR-302/372/373/520 in invasive pituitary tumors. Cell Physiol. Biochem. *48*, 1291–1303. https://doi.org/10.1159/000492089.
20. Zhou, Z., and Huang, F. (2019). Long non-coding RNA LINC00152 regulates cell proliferation, migration and invasion in esophageal squamous cell carcinoma via miR-107/Rab10 Axis. Onco Targets Ther. *12*, 8553–8567. https://doi.org/10.2147/OTT.S221515.
21. Zhang, Z., Cheng, J., Wu, Y., Qiu, J., Sun, Y., and Tong, X. (2016). LncRNA HOTAIR controls the expression of Rab22a by sponging miR-373 in ovarian cancer. Mol. Med. Rep. *14*, 2465–2472. https://doi.org/10.3892/mmr.2016.5572.
22. Wang, Z., Zhao, Y., Xu, N., Zhang, S., Wang, S., Mao, Y., Zhu, Y., Li, B., Jiang, Y., Tan, Y., et al. (2019). NEAT1 regulates neuroglial cell mediating Aβ clearance via the epigenetic regulation of endocytosis-related genes expression. Cell Mol. Life Sci. *76*, 3005–3018. https://doi.org/10.1007/s00018-019-03074-9.
23. Wang, X., Li, L., Zhao, K., Lin, Q., Li, H., Xue, X., Ge, W., He, H., Liu, D., Xie, H., et al. (2020). A novel LncRNA HITT forms a regulatory loop with HIF-1α to modulate angiogenesis and tumor growth. Cell Death. Differ. *27*, 1431–1446. https://doi.org/10.1038/s41418-019-0449-8.
24. Wang, X., Wang, Y., Li, L., Xue, X., Xie, H., Shi, H., and Hu, Y. (2020). A lncRNA coordinates with Ezh2 to inhibit HIF-1α transcription and suppress cancer cell adaption to hypoxia. Oncogene *39*, 1860–1874. https://doi.org/10.1038/s41388-019-1123-9.
25. Ramalingam, S.S., Owonikoko, T.K., and Khuri, F.R. (2011). Lung cancer: new biological insights and recent therapeutic advances. CA Cancer J. Clin. *61*. https://doi.org/10.3322/caac.20102.
26. Zhang, P.-F., Zeng, G.-Q., Yi, L.-Z., Liu, J.-P., Wan, X.-X., Qu, J.-Q., Li, J.-H., Li, C., Tang, C.-E., Hu, R., et al. (2013). Identification of integrin β1 as a prognostic biomarker for human lung adenocarcinoma using 2D-LC-MS/MS combined with iTRAQ technology. Oncol. Rep. *30*, 341–349. https://doi.org/10.3892/or.2013.2477.
27. Diggins, N.L., Kang, H., Weaver, A., and Webb, D.J. (2018). α5β1 integrin trafficking and Rac activation are regulated by APPL1 in a Rab5-dependent manner to inhibit cell migration. J. Cell Sci. *131*. https://doi.org/10.1242/jcs.207019.
28. Delprato, A., Merithew, E., and Lambright, D.G. (2004). Structure, exchange determinants, and family-wide rab specificity of the tandem helical bundle and Vps9 domains of Rabex-5. Cell *118*, 607–617.
29. Fares, J., Fares, M.Y., Khachfe, H.H., Salhab, H.A., and Fares, Y. (2020). Molecular principles of metastasis: a hallmark of cancer revisited. Signal. Transduct. Target Ther. *5*, 28. https://doi.org/10.1038/s41392-020-0134-x.
30. Mendoza, P., Díaz, J., Silva, P., and Torres, V.A. (2014). Rab5 activation as a tumor cell migration switch. Small GTPases *5*, e28195. https://doi.org/10.4161/sgtp.28195.
31. Zhang, Y., Tang, P.M.-K., Niu, Y., García Córdoba, C.A., Huang, X.-R., Yu, C., and Lan, H.-Y. (2020). Long non-coding RNA LRNA9884 promotes acute kidney injury via regulating NF-kB-Mediated transcriptional activation of MIF. Front. Physiol. *11*, 590027. https://doi.org/10.3389/fphys.2020.590027.
32. Zhang, Y.-Y., Tang, P.M.-K., Tang, P.C.-T., Xiao, J., Huang, X.-R., Yu, C., Ma, R.C.W., and Lan, H.-Y. (2019). LRNA9884, a novel Smad3-dependent long noncoding RNA, promotes diabetic kidney injury in/mice via enhancing MCP-1-dependent renal inflammation. Diabetes *68*, 1485–1498. https://doi.org/10.2337/db18-1075.
33. Mattera, R., and Bonifacino, J.S. (2008). Ubiquitin binding and conjugation regulate the recruitment of Rabex-5 to early endosomes. EMBO J. *27*, 2484–2494. https://doi.org/10.1038/emboj.2008.177.
34. Shideler, T., Nickerson, D.P., Merz, A.J., and Odorizzi, G. (2015). Ubiquitin binding by the CUE domain promotes endosomal localization of the Rab5 GEF Vps9. Mol. Biol. Cell *26*, 1345–1356. https://doi.org/10.1091/mbc.E14-06-1156.
35. Kim, H., Oh, H., Oh, Y.S., Bae, J., Hong, N.H., Park, S.J., Ahn, S., Lee, M., Rhee, S., Lee, S.H., et al. (2019). SPIN90, an adaptor protein, alters the proximity between Rab5 and Gapex5 and facilitates Rab5 activation during EGF endocytosis. Exp. Mol. Med. *51*, 85. https://doi.org/10.1038/s12276-019-0284-5.
36. Pan, J.Y., Sanford, J.C., and Wessling-Resnick, M. (1995). Effect of guanine nucleotide binding on the intrinsic tryptophan fluorescence properties of Rab5. J. Biol. Chem. *270*, 24204–24208.
37. Shin, D., Na, W., Lee, J.-H., Kim, G., Baek, J., Park, S.H., Choi, C.Y., and Lee, S. (2017). Site-specific monoubiquitination downregulates Rab5 by disrupting effector binding and guanine nucleotide conversion. Elife *6*. https://doi.org/10.7554/eLife.29154.
38. Zhao, K., Wang, X., Xue, X., Li, L., and Hu, Y. (2020). A long noncoding RNA sensitizes genotoxic treatment by attenuating ATM activation and homologous recombination repair in cancers. PLoS Biol. *18*, e3000666. https://doi.org/10.1371/journal.pbio.3000666.
39. Ryan, M.B., and Corcoran, R.B. (2018). Therapeutic strategies to target RAS-mutant cancers. Nat. Rev. Clin. Oncol. *15*, 709–720. https://doi.org/10.1038/s41571-018-0105-0.
40. Imielinski, M., Berger, A.H., Hammerman, P.S., Hernandez, B., Pugh, T.J., Hodis, E., Cho, J., Suh, J., Capelletti, M., Sivachenko, A., et al. (2012). Mapping the hallmarks of lung adenocarcinoma with massively parallel sequencing. Cell *150*, 1107–1120. https://doi.org/10.1016/j.cell.2012.08.029.
41. Cancer Genome Atlas Research, N. (2014). Comprehensive molecular profiling of lung adenocarcinoma. Nature *511*, 543–550. https://doi.org/10.1038/nature13385.
42. Barbieri, M.A., Kohn, A.D., Roth, R.A., and Stahl, P.D. (1998). Protein kinase B/akt and rab5 mediate Ras activation of endocytosis. J. Biol. Chem. *273*, 19367–19370.
43. Stein, M.-P., Dong, J., and Wandinger-Ness, A. (2003). Rab proteins and endocytic trafficking: potential targets for therapeutic intervention. Adv. Drug Deliv. Rev. *55*, 1421–1437.
44. Qin, X., Wang, J., Wang, X., Liu, F., Jiang, B., and Zhang, Y. (2017). Targeting Rabs as a novel therapeutic strategy for cancer therapy. Drug Discov. Today *22*, 1139–1147. https://doi.org/10.1016/j.drudis.2017.03.012.
45. Hammerling, B.C., Najor, R.H., Cortez, M.Q., Shires, S.E., Leon, L.J., Gonzalez, E.R., Boassa, D., Phan, S., Thor, A., Jimenez, R.E., et al. (2017). A Rab5 endosomal pathway mediates Parkin-dependent mitochondrial clearance. Nat. Commun. *8*, 14050. https://doi.org/10.1038/ncomms14050.

46. Kitano, M., Nakaya, M., Nakamura, T., Nagata, S., and Matsuda, M. (2008). Imaging of Rab5 activity identifies essential regulators for phagosome maturation. Nature *453*, 241–245. https://doi.org/10.1038/nature06857.

47. Zeigerer, A., Bogorad, R.L., Sharma, K., Gilleron, J., Seifert, S., Sales, S., Berndt, N., Bulik, S., Marsico, G., D'Souza, R.C.J., et al. (2015). Regulation of liver metabolism by the endosomal GTPase Rab5. Cell Rep. *11*, 884–892. https://doi.org/10.1016/j.celrep.2015.04.018.

48. Xu, W., Fang, F., Ding, J., and Wu, C. (2018). Dysregulation of Rab5-mediated endocytic pathways in Alzheimer's disease. Traffic *19*, 253–262. https://doi.org/10.1111/tra.12547.

49. Hermle, T., Schneider, R., Schapiro, D., Braun, D.A., van der Ven, A.T., Warejko, J.K., Daga, A., Widmeier, E., Nakayama, M., Jobst-Schwan, T., et al. (2018). Mutations implicate RAB5 regulation in nephrotic syndrome. J. Am. Soc. Nephrol. *29*, 2123–2138. https://doi.org/10.1681/ASN.2017121312.